Geological Society, London, Special Publications

Tsunami hazard related to a flank collapse of Anak Krakatau Volcano, Sunda Strait, Indonesia

T. Giachetti, R. Paris, K. Kelfoun and B. Ontowirjo

Geological Society, London, Special Publications 2012, v.361; p79-90.
doi: 10.1144/SP361.7

Notes

Tsunami hazard related to a flank collapse of Anak Krakatau Volcano, Sunda Strait, Indonesia

T. GIACHETTI[1,3]*, R. PARIS[2,4,6], K. KELFOUN[2,4,6] & B. ONTOWIRJO[5]

[1]*Clermont Université, Université Blaise Pascal, Geolab, BP 10448, F-63000 Clermont-Ferrand, France*

[2]*Clermont Université, Université Blaise Pascal, Laboratoire Magmas et Volcans, BP 10448, F-63000 Clermont-Ferrand, France*

[3]*CNRS, UMR 6042, Geolab, F-63057 Clermont-Ferrand, France*

[4]*CNRS, UMR 6524, LMV, F-63038 Clermont-Ferrand, France*

[5]*Coastal Dynamics Research Center, BPDP-BPPT, 11th Floor, Building 2, BPPT, Jl, M. H. Thamrin no 8, Jakarta 10340, Indonesia*

[6]*IRD, R 163, LMV, F-63038 Clermont-Ferrand, France*

**Corresponding author (e-mail: giachettithomas@club-internet.fr)*

Abstract: Numerical modelling of a rapid, partial destabilization of Anak Krakatau Volcano (Indonesia) was performed in order to investigate the tsunami triggered by this event. Anak Krakatau, which is largely built on the steep NE wall of the 1883 Krakatau eruption caldera, is active on its SW side (towards the 1883 caldera), which makes the edifice quite unstable. A hypothetical 0.280 km^3 flank collapse directed southwestwards would trigger an initial wave 43 m in height that would reach the islands of Sertung, Panjang and Rakata in less than 1 min, with amplitudes from 15 to 30 m. These waves would be potentially dangerous for the many small tourist boats circulating in, and around, the Krakatau Archipelago. The waves would then propagate in a radial manner from the impact region and across the Sunda Strait, at an average speed of 80–110 km h^{-1}. The tsunami would reach the cities located on the western coast of Java (e.g. Merak, Anyer and Carita.) 35–45 min after the onset of collapse, with a maximum amplitude from 1.5 (Merak and Panimbang) to 3.4 m (Labuhan). As many industrial and tourist infrastructures are located close to the sea and at altitudes of less than 10 m, these waves present a non-negligible risk. Owing to numerous reflections inside the Krakatau Archipelago, the waves would even affect Bandar Lampung (Sumatra, *c.* 900 000 inhabitants) after more than 1 h, with a maximum amplitude of 0.3 m. The waves produced would be far smaller than those occurring during the 1883 Krakatau eruption (*c.* 15 m) and a rapid detection of the collapse by the volcano observatory, together with an efficient alert system on the coast, would possibly prevent this hypothetical event from being deadly.

Most recorded historical tsunamis have a seismic origin, but such events may also be triggered by phenomena related to huge volcanic eruptions, such as large pyroclastic flows entering the water (e.g. de Lange *et al.* 2001; Maeno & Imamura 2007), submarine explosions (e.g. Mader & Gittings 2006), caldera collapse (e.g. Nomanbhoy & Satake 1995; Maeno *et al.* 2006) or by a large, rapidly sliding mass impacting the water (e.g. Tinti *et al.* 1999, 2000, 2006; Keating & McGuire 2000; Ward 2001; Harbitz *et al.* 2006; Fritz *et al.* 2008; Waythomas *et al.* 2009; Kelfoun *et al.* 2010). The December 2002 17×10^6 m^3 flank collapse of Stromboli triggered a 8 m-high run-up on the coast of Stromboli, but had little effect on coasts located more than 200 km from the collapse (Maramai *et al.* 2005). The tsunami generated by the 30×10^6 m^3 Lituya Bay collapse in Alaska in 1958 (Fritz *et al.* 2001) reached 60 m at 6 km laterally from the collapse and 30 m at 12 km. These tsunamis had very few fatalities as they occurred either in isolated locations (Lituya Bay, Alaska) or during a period of no tourist activity (Stromboli). The largest lateral collapse of an island volcano recorded in historical times (*c.* 5 km^3) took place during the 1888 eruption of Ritter Island (New Guinea), producing witnessed waves of up to 10–15 m at tens to hundreds of kilometres from the source (Ward & Day 2003). With 15 000 fatalities, the tsunami generated by the 1792 sector collapse of Mount

From: TERRY, J. P. & GOFF, J. (eds) 2012. *Natural Hazards in the Asia–Pacific Region: Recent Advances and Emerging Concepts*. Geological Society, London, Special Publications, **361**, 79–90, http://dx.doi.org/10.1144/SP361.7

Mayuyama in Ariake Bay (Kyushu Island, Unzen volcanic complex) was the second worst disaster in Japan, and the second deadliest volcanic tsunami (after that produced by the eruption of Krakatau in 1883). The failure was most probably triggered by a strong earthquake, and its volume was about 340×10^6 m^3 (Michiue *et al.* 1999). Tsunami run-ups ranged from 8 to 24 m on the opposite side of Ariake Bay (Tsuji & Hino 1993).

The 26–28 August 1883 Plinian eruption of Krakatau Volcano, and its subsequent tsunamis, caused more than 35 000 casualties along the coasts of the Sunda Strait in Indonesia (Self & Rampino 1981; Simkin & Fiske 1983; Sigurdsson *et al.* 1991*a*, *b*). This eruption was one of the most powerful and devastating eruptions in recorded history. Many tsunamis were produced during this approximately 2 day eruption, the largest one occurring after 10 a.m. on the 27 August (Warton & Evans 1888; Yokoyama 1981). The leading wave reached the cities of Anyer and Merak on Java after 35–40 min, and after approximately 1 h for the city of Bandar Lampung (Teluk Betung) on Sumatra. A tide gauge located near Jakarta (Batavia Harbour, Java) registered the wave arrival approximately 140 min after its inferred initiation at Krakatau Island. Using the tsunami run-ups determined along the coasts of Java and Sumatra (Verbeek 1885), the tsunami heights before run-up were estimated to be about 15 m at the coastline all around the Sunda Strait (Symons 1888). The generation mechanism of these 1883 tsunamis is still controversial and several processes may have acted successively or together (Self & Rampino 1981; Yokoyama 1981; Camus & Vincent 1983; Francis 1985). Based on low-resolution numerical simulations, Nomanbhoy & Satake (1995) concluded that a series of submarine explosions over a period of 1–5 min was the most probable source for the major tsunami. Nevertheless, pyroclastic flows formed by the gravitational collapse of the eruptive columns are also a possible source for most of the tsunamis observed before and during the paroxysm (Carey *et al.* 1996; de Lange *et al.* 2001).

Nearly 45 years after this 1883 cataclysmal eruption, Anak Krakatau ('Child of Krakatau' in Indonesian) emerged from the sea in the same location as the former Krakatau, and has since grown to its current height of more than 300 m (Hoffmann-Rothe *et al.* 2006). It exhibits frequent activity, still posing a risk to the coastal population of Java and Sumatra, and for the important shipping routes through the Sunda Strait. Following the active phase of Anak Krakatau in 1980, a permanent volcano observatory was established in Pasauran on the western coast of Java, about 50 km east of the Krakatau Archipelago. A short-period seismometer placed on the volcano flank, visual control and daily seismic event statistics are used to determine the current alert level, on the basis of which Indonesian authorities decide about preventive measures, sometimes prohibiting tourism around the archipelago (Hoffmann-Rothe *et al.* 2006).

One possible major hazard emerging from Anak Krakatau would be a tsunami triggered by a collapse of its flank, as the volcano is partly built on a steep wall of the caldera resulting from the 1883 eruption. A small tsunami (*c.* 2 m high) was experienced on Rakata Island in October 1981 during an awakening of Anak Krakatau (Camus *et al.* 1987). In the present study, we numerically simulate a sudden southwestwards destabilization of a large part of the Anak Krakatau Volcano, and the subsequent tsunami formation and propagation. We show results concerning the time of arrival and the amplitude of the waves produced, both in the Sunda Strait and on the coasts of Java and Sumatra. We then discuss the relationships between the morphology of Anak Krakatau, the locations of the surrounding islands, the bathymetry of the strait and the triggered waves.

Geography, population and infrastructures in the Sunda Strait

The Sunda Strait, in which Anak Krakatau Volcano lies, has a roughly NE–SW orientation, with a minimum width of 24 km at its NE end between Sumatra and Java (Fig. 1). Its western end is deep (< -1500 m), but it shallows significantly as it narrows to the east, with a depth of only about 20 m in parts of the eastern end, making it difficult to navigate due to sandbanks and strong tidal flows. The numerous islands in the strait and the nearby surrounding regions of Java and Sumatra were devastated by the 1883 Krakatau eruption. The eruption drastically altered the topography of the strait, with approximately 12 km^3 (DRE, dense rock equivalent) of ignimbrite being deposited around the volcano (Carey *et al.* 1996). The small to moderate volcanic explosions of Anak Krakatau, which is partly built on the site of the former Krakatau Island, attract tourist boats that circulate between the islands of the Krakatau Archipelago.

Some areas have never been resettled since the 1883 eruption (e.g. the SW of Java), but much of the coastline is now densely populated, especially in Bandar Lampung (*c.* 900 000 inhabitants) on Sumatra, and on the west coast of the Cilegon District (*c.* 400 000 inhabitants) in Java (Fig. 1). Moreover, many of the roads on western Java and southern Sumatra are located near the sea and at low altitude (< 10 m), as well as important economic infrastructures such as power stations (e.g. Labuhan, NE of Merak and SE of Banda

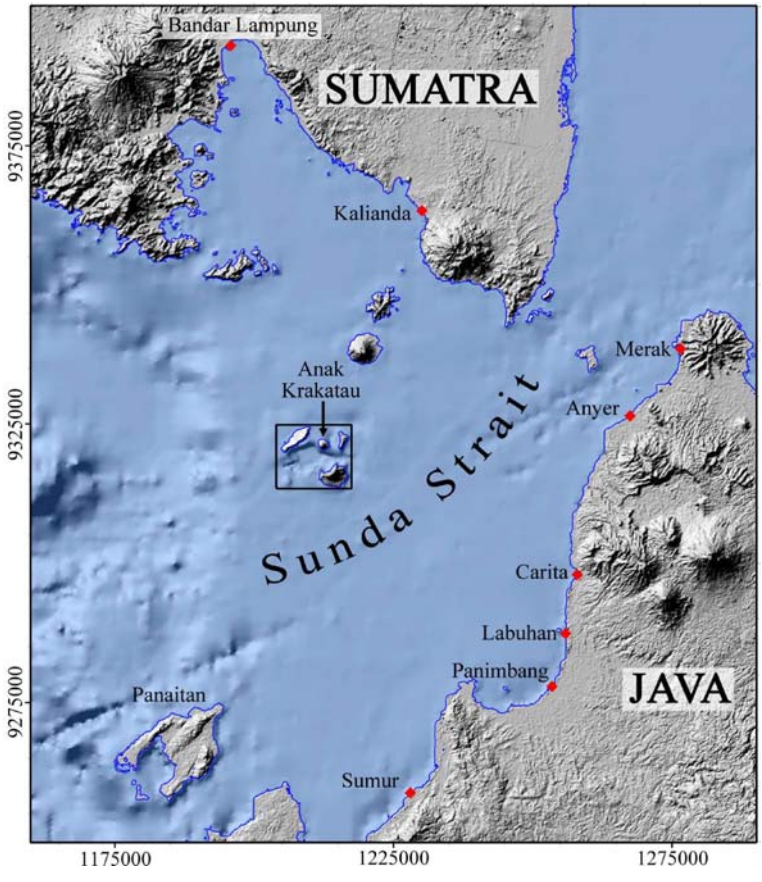

Fig. 1. Shaded relief representation of the DEM (100 m resolution) of Sunda Strait, based on ASTER topography, GEBCO bathymetry and a digitization of the bathymetric map of Krakatau from Deplus *et al.* (1995, their fig. 7). This DEM is the calculation grid used to simulate the Anak Krakatau landslide and the subsequent tsunami propagation (calculations were made at a resolution of 200 m). The main coastal cities or important infrastructures around the Sunda Strait are indicated by red diamonds. The black frame around the Krakatau Archipelago corresponds to the limits of Figure 2b, c. Geographical co-ordinates are in metres.

Lampung), industries (e.g. steel industries in Cilegon), major harbours connecting Java and Sumatra (Merak, Bakaheuni), and tourist resorts (e.g. Anyer, Kalianda). There are also several oil platforms in the strait, notably off the Java coast. Such infrastructures would potentially be badly affected by a tsunami of several metres, as was produced during the 1883 eruption.

In October 2007, the Indonesian government planned the construction of a 30 km road and railway connection between the islands of Sumatra and Java (the Selat Sunda Bridge), across the 26 km Sunda Strait, at an altitude of 70 m asl (above sea level). In 2009, the 'pre-feasibility' study for this 10 billion dollar project was completed and the construction is expected to begin in 2012. Owing to the seismic and volcanic activity in the Sunda region, this project faces many challenges. Krakatau Volcano is located only 40 km away from the future bridge. Some of the bridge's piles may suffer from tsunamis crossing the Sunda Strait, therefore such hazards need to be quantified.

Anak Krakatau Volcano: evolution and actual morphology

Anak Krakatau first rose up out of the sea in 1928, sited just off the steep NE wall of the basin formed by the collapse of the 1883 Krakatau eruption caldera. This volcano was built where the main vent for the 1883 eruption is supposed to have been located, about midway between the former craters of Danan and Perbuatan (Deplus

et al. 1995). Between 1928 and 1930, the volcano receded and reappeared three times until it established itself permanently above sea level. In 1959, an uninterrupted 152 m-high hyaloclastic tuff-ring developed (Sudradjat 1982) and a lake formed in the crater. The eruption style was Surtseyan during the 1928–1930 period (Stehn 1929; Camus *et al.* 1987), then Vulcanian until 1960, before shifting to Strombolian explosions that created a cone reaching 200 m asl in 1981 (Oba *et al.* 1983). In 1981, a Vulcanian eruption marked a southwestwards shift of Anak Krakatau activity (Sudrajat 1982) with more differentiated volcanic products (acid andesites, dacites) than previously erupted (mainly basalts and andesites before 1981: Camus *et al.* 1987). At the time of writing, the latest eruption of Anak Krakatau, which started on 25 October 2010, is still ongoing, with dense ash clouds forming plumes 100–1000 m high.

Rapid soundings in 1928 have shown that the western slope of the volcano was considerably steeper ($>28^{\circ}$) than the eastern, as a consequence of its position on the steep wall of the basin and also of the strong current that is generally running from SW to NE (Stehn 1929). Deplus *et al.* (1995) showed that this slope was still in existence in 1995, and that the successive eruptions had not resulted in an infilling of the caldera. According to these data concerning the steep slopes on which Anak Krakatau is built and the fact that this volcano is growing towards the SW, landslides along its southwestern flank cannot be excluded (Deplus *et al.* 1995). Such a landslide would be directed southwestwards into the 1883 caldera and would trigger waves that would propagate into the Sunda Strait, possibly affecting the Indonesian coasts.

Methodology

Digital elevation model used and scenario envisaged

The collapse of the Anak Krakatau Volcano was simulated on a digital elevation model (DEM) obtained by merging the ASTER (*Advanced Spaceborne Thermal Emission and Reflection* Radiometer) topography (*c.* 30 m resolution), bathymetric maps (one from Dishidros Indonesian Navy and a Sunda Strait navigation chart) and the GEBCO (General Bathymetric Chart of the Oceans) bathymetry (*c.* 900 m resolution) of the whole Sunda Strait region (Fig. 1). In addition, the bathymetric map of the Krakatau Archipelago from Deplus *et al.* (1995, their fig. 7) was digitized and added to the DEM in order to obtain a better resolution of the zone where the collapse occurs and where the waves are initially produced (Fig. 2b). The final DEM produced, which is the calculation grid used for the numerical simulation, is a 1500×1300 pixel grid with a spatial resolution of 100 m (Fig. 1). In order to maximize on the best spatial resolution available to register the initial waves produced, some of the simulations were performed on a portion of the grid centred on the landslide event. Owing to the long calculation times we down-sampled the grid by a factor of 2 (i.e. 750×650 pixel calculation grid and a spatial resolution of 200 m) for the simulations of tsunami propagation over the entire Sunda Strait area.

Some level lines of the DEM were modified to build the sliding surface of the hypothetical landslide; that is, to define the hypothetical collapse scar. This was done so that: (1) the upper end of the scar is broadly defined by the limit between the older tuff-ring and the new cone (Fig. 2a, c); (2) the base of the scar lies at the bottom of the 1883 caldera (Fig. 2a); and (3) the scar is horseshoe-shaped (Fig. 2c). The scar is oriented southwestwards, with an average slope of 8.2° (Fig. 2a) and a width of *c.* 1.9 km, defining a collapsing volume of 0.280 km^3. This scar probably cuts the NE wall of the 1883 caldera, but this cannot be clearly traced on the DEM as no precise bathymetric data immediately following the 1883 eruption are available. In our simulation, the debris avalanche is released in a single event.

Numerical model

We used the numerical code *VolcFlow* (Kelfoun *et al.* 2010; Giachetti *et al.* 2011) to simulate both the Anak Krakatau landslide and the tsunami propagations. A full explanation of the code and equations is given in the previously cited papers. This code is based on the two-dimensional (2D) depth-average approach, modified to incorporate 3D interactions with greater accuracy; both the landslide and the sea water being simulated using the general shallow-water equations of mass conservation and momentum balance. In the model, the water interacts with the bathymetry/topography and floods onto the land, but waves breaking and other complex second-order 3D effects are not taken into account, and sediment erosion and transport are also ignored.

We simulated the water propagation using a density of 1000 kg m^{-3} and a viscosity of 0.001 Pa s. As emissions from Anak Krakatau are mainly composed of scoriaceous material with a basaltic (common) to dacitic (rarer) chemical composition (Sudradjat 1982; Camus *et al.* 1987), we used a density of 1500 kg m^{-3} to simulate the landslide. Kelfoun *et al.* (2010) and Giachetti *et al.* (2011) showed that the rheology used to simulate the landslide propagation may be important when dealing with second-order variations of the profile

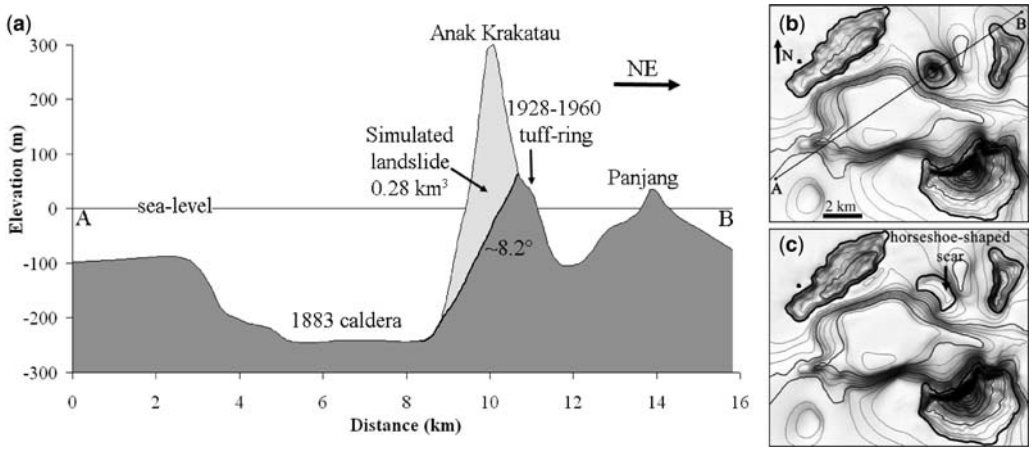

Fig. 2. (**a**) Cross-section of Anak Krakatau (inset: Fig. 1) and the 1883 eruption caldera. The landslide scar, defined by modifying some level lines on our initial DEM, is drawn in black. It is orientated southwestwards, with a slope of 8.2°, delimiting a collapsing volume of about 0.28 km^3. (**b**) Topography before the simulated landslide, with the location of the cross-section presented in (a). The caldera resulting from the 1883 Krakatau eruption is clearly visible, as well as Anak Krakatau, which is built on the NE flank of this caldera. (**c**) Topography after the simulated landslide, with the horseshoe-shaped scar clearly visible.

and amplitude of the triggered waves. Thus, we tested four sets of rheological parameters to simulate the debris avalanche propagation: a commonly used Mohr–Coulomb frictional law with a basal friction angle of 1° or 2° (hereafter referred to as rheologies 1 and 2, respectively) and a constant retarding stress of 5 or 10 kPa (rheologies 3 and 4, respectively). Although the Mohr–Coulomb frictional law is often used in granular-flow dynamics because it represents the behaviour of deposits at rest and of sand flows in the laboratory, the constant retarding stress appears to be better adapted to the reproduction of the extent, thickness on all slopes and some morphological features of natural deposits (e.g. Dade & Huppert 1998; Kelfoun & Druitt 2005). Figure 3a shows that the surface area covered by the simulated debris avalanche deposits varies depending on the rheology used (the numerical deposits obtained using rheologies 1–2 and rheologies 3–4 are quasi-identical and are thus drawn together). Figure 3b presents the water surface displacement recorded using a gauge placed approximately 15 km southwestwards from the landslide scar (black diamond in Fig. 3a), in

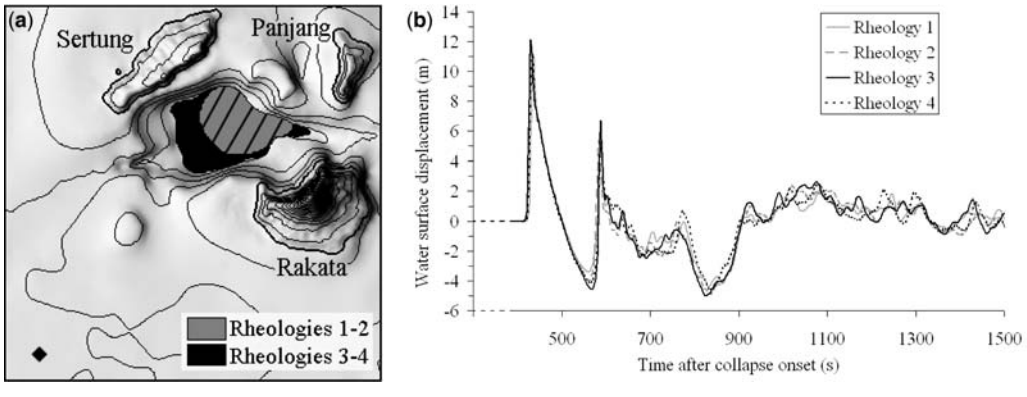

Fig. 3. (**a**) Simulated debris avalanche deposits obtained using rheologies 1–2 (grey) and 3–4 (black hatching and black) to simulate the landslide propagation. (**b**) Simulated water surface displacement recorded at the gauge located in Figure 2a (black diamond). This figure shows that the waves produced are very similar, whatever the rheology used to simulate the landslide propagation.

the direction of propagation of the major triggered waves, where the water depth is aproximately 100 m. It shows that the wave profiles and amplitudes created are very similar, whichever of the four rheologies are used. The maximum amplitude recorded at the gauge placed approximately 15 km southwestwards varies between 11 (rheology 2) and 12 m (rheology 3).

We believe that the similarity between the wave profiles presented in Figure 3b is due to the initial geometry of the collapsing volume and the landslide scar. Indeed, as the collapsing volume is initially partly submerged and the landslide scar directs the debris avalanche southwestwards, the initial waves triggered by the landslide–water impact are poorly influenced by the rheology used to simulate landslide propagation. This rheology, however, plays a role in the final run-out of the modelled debris avalanche deposits (Fig. 3a). The morphology of the modelled deposits (not shown here) is very similar whatever the rheology used because of the dominant controlling factor of the structure of the 1883 caldera. The rheology used to simulate the landslide propagation is also responsible for the small second-order discrepancies existing between the wave profiles registered, which are amplified over time (Fig. 3b). However, since in this paper we focus on the tsunami hazards and not on the simulated morphology of the debris avalanche deposits, we arbitrarily chose the constant retarding stress of 10 kPa (rheology 4) to simulate the landslide propagation for the whole calculation grid.

Results

When interacting with the water, the debris avalanche triggers waves whose maximum initial amplitude is around 45 m, measured approximately 45 s after the collapse onset at 2.5 km southwestwards from the landslide scar. The waves produced then propagate in a radial manner away from the impact region, reaching the islands of Sertung, Panjang and Rakata (Fig. 3a) in less than 1 min, with amplitudes from 15 to 30 m. Owing to the southwestwards propagation of the landslide, the highest waves are produced in this direction. The wave profile obtained about 15 km SW from the landslide scar (Fig. 3b, rheology 4) shows a first wave with an amplitude of 11.3 m and a period of around 162 s (wavelength of c. 3.4 km). This is followed by another 5.3 m wave, with a smaller period of approximately 60 s (wavelength of c. 1.3 km). This is then followed by several smaller and shorter waves, the sea level regaining its initial position after a few tens of minutes. The travel time of the first wave is shown in Figure 4, and is given more precisely in Table 1 for the main coastal cities and infrastructures located in Figure 1. The cities situated on the western coast of Java are all touched by the first wave between 36 and 47 min after the onset of the Anak Krakatau collapse. The first wave reaches Kalianda and Bandar Lampung, located on Sumatra, 45 and 68 min after the onset of the collapse, respectively. Note that everywhere in the Sunda Strait the wavelength of the simulated waves is always more than 25 times the water depth. This demonstrates that the use of the general shallow-water equations of mass conservation and momentum balance to simulate the water propagation is appropriate in this case (e.g. Synolakis *et al.* 1997).

Figure 5 presents the maximum wave amplitude registered over 6000 s of simulation. It shows that the highest waves are mainly concentrated around

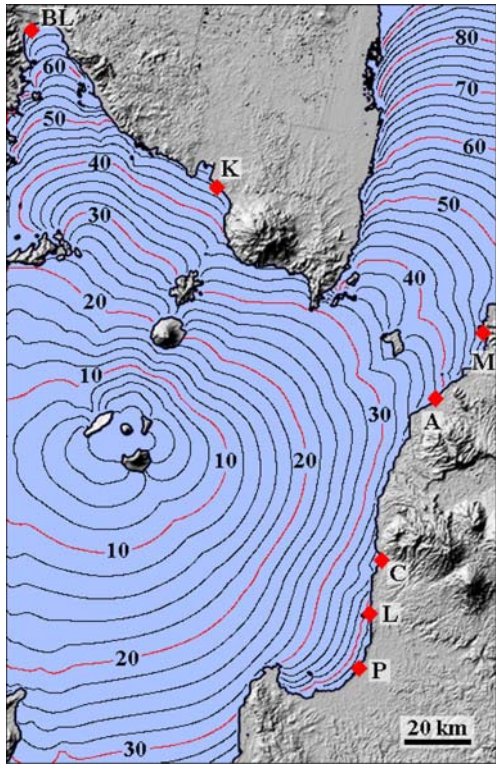

Fig. 4. First wave travel time (expressed in min) for the first 90 min of simulation. Black lines are at 2 min intervals. Main coastal cities (names in Fig. 1) are shown by red diamonds. The impact of the sudden increase in water depth westwards from the Krakatau Archipelago is clearly seen (see Fig. 1 for bathymetry), the waves being more rapid than those crossing the shallow strait. BL, Bandar Lampung; K, Kalianda; M, Merak; A, Anyer; C, Carita; L, Labuhan; P, Panimbang. The simulation of the landslide propagation was carried out using a constant retarding stress of 10 kPa.

Table 1. *Travel time and maximum wave amplitude recorded at gauges located close (<900 m) to the main coastal cities of the Sunda Strait (see Fig. 1)*

	Bandar Lampung (−13 m)	Kalianda (−5 m)	Merak (−12 m)	Anyer (−12 m)	Carita (−12 m)	Labuhan (−4 m)	Panimbang (−2 m)	Sumur (−7 m)
Travel time (min)	68	44	47	38	37	40	43	36
Maximum wave amplitude (m)	0.3	2.7	1.5	1.4	2.9	3.4	1.5	1.2

For each city, the initial water depth at the gauge site is given in brackets.

the Krakatau Archipelago, as it is the location of the triggering event, and their amplitude logically decreases away from Anak Krakatau. Westwards, at about 20 km from the landslide, the wave amplitude is slightly reduced because of the strong increase in water depth, and waves do not exceed 1–2 m when they reach the western edge of the calculation grid. The highest waves produced are directed southwestwards and their amplitude decreases when they reach greater water depths in the SW. However, they still have an amplitude of more than 3–4 m when they arrive near Panaitan and near the southwestern coast of Java (Ujung Kulon National Park). The presence of the islands of Sertung and Rakata (Fig. 3a) – NW and SW of the landslide, respectively – also causes the wave amplitude to be reduced. The maximum amplitude of the waves recorded northwards and northeastwards is not related to the first wave produced. It appears that they come from the reflection of the initial waves off the coasts of Sertung and Rakata (the former consisting of a high cliff orientated NNW). However, owing to the numerous interactions of the waves with the four islands of the Krakatau Archipelago, it is difficult to establish exactly what happens near the impact point. Figure 5 also shows some reflections of the waves, in particular off the western coast of Java.

Figure 6 presents the evolution of the water level over 6500 s of simulation, recorded at gauges placed in the sea a few hundreds of metres (<900 m) off eight of the main coastal cities or infrastructures of the Sunda Strait (located in Fig. 1). The gauges were placed in the sea near the coasts to free the sea-level profiles recorded from the 3D interactions that the program fails to reproduce in an accurate manner. The maximum wave amplitudes measured at these gauges are indicated in Table 1 (the vertical water depth at each gauge is indicated in Table 1). The water-level profiles are different from one city to another, being complicated by numerous reflections of the waves throughout the Krakatau Archipelago, as well as around the Sumatran and Javanese coasts. All of the cities are touched by a first positive wave with amplitude ranging from 0.3 to 2.3 m, but this first wave is never the highest one. Near Bandar Lampung and Kalianda, the maximum wave amplitude measured is 0.3 and 2.7 m respectively, and the coastal cities of western Java are generally affected by waves with maximums of between 1.2 (Sumur) and 3.4 m (Labuhan).

Discussion

Influence of the initial parameters on the wave characteristics

The volume of a debris avalanche and the way it occurs (e.g. in one go, by retrogressive failures) are the parameters that most influence the characteristics of the triggered tsunami (Locat *et al.* 2004; Giachetti *et al.* 2011). In the present case, the hypothetical scar has a slope of 8.2°, for an initial Anak Krakatau average slope of 24.2° (Fig. 3a). These values are lower than those observed for other scars of debris avalanches that triggered tsunamis, like the Palos Verdes debris avalanche (California, scar slope of 10°–17°: Locat *et al.* 2004) or 29 submarine events identified at Stromboli (average scar slope of *c*. 25°, and pre-failure slope of *c*. 28° for debris avalanches between 5 and 200 m b.s.l.: Casalbore *et al.* 2011). In this study, we decided to base the structural definition of the hypothetical scar on the known structural evolution of Anak Krakatau: the upper end of the scar being defined by the limit between the older tuff-ring and the new cone, and its base by the bottom of the 1883 caldera. Therefore, our numerical model of Anak Krakatau involves a debris avalanche volume of 0.280 km^3. The definition of a steeper scar (closer to the values observed by Locat *et al.* 2004 or Casalbore *et al.* 2011) would lead to a more rapid landslide into the water, and thus possibly to higher waves. However, a steeper scar would also result in a smaller collapsing volume (considering the lower end of the scar as fixed) and thus to slightly smaller waves. Since in this study our aim is to quantify the tsunami hazard linked to a realistic partial flank collapse of Anak Krakatau, we decided to maximize the volume involved in the debris avalanche (and

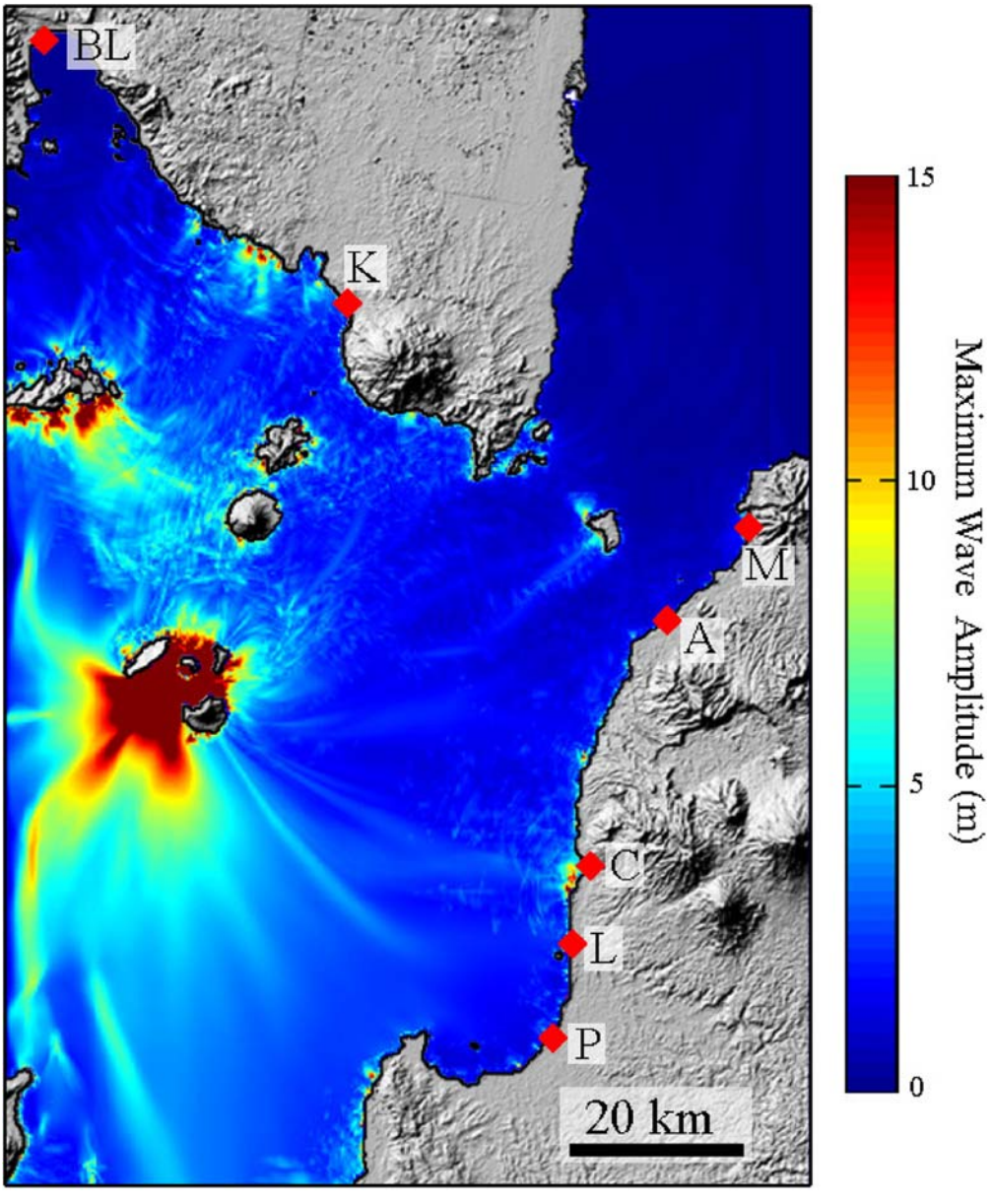

Fig. 5. Maximum wave amplitude (m) recorded over 6000 s of simulation, using a constant retarding stress of 10 kPa to simulate the landslide propagation.

thus the waves produced) while remaining consistent with the structure of the volcano.

Influence of the bathymetry/topography on the tsunami characteristics

To define the initial volume that would hypothetically collapse, we used the available topography data (ASTER data, spatial resolution of 30 m) for Anak Krakatau Island. However, there is no up-to-date high-resolution topography and bathymetry data for this volcano, whose morphology changes rapidly due to its numerous eruptions. For this reason, we think that high-resolution topographical and bathymetric surveys of the Anak Krakatau Volcano should be performed in order to

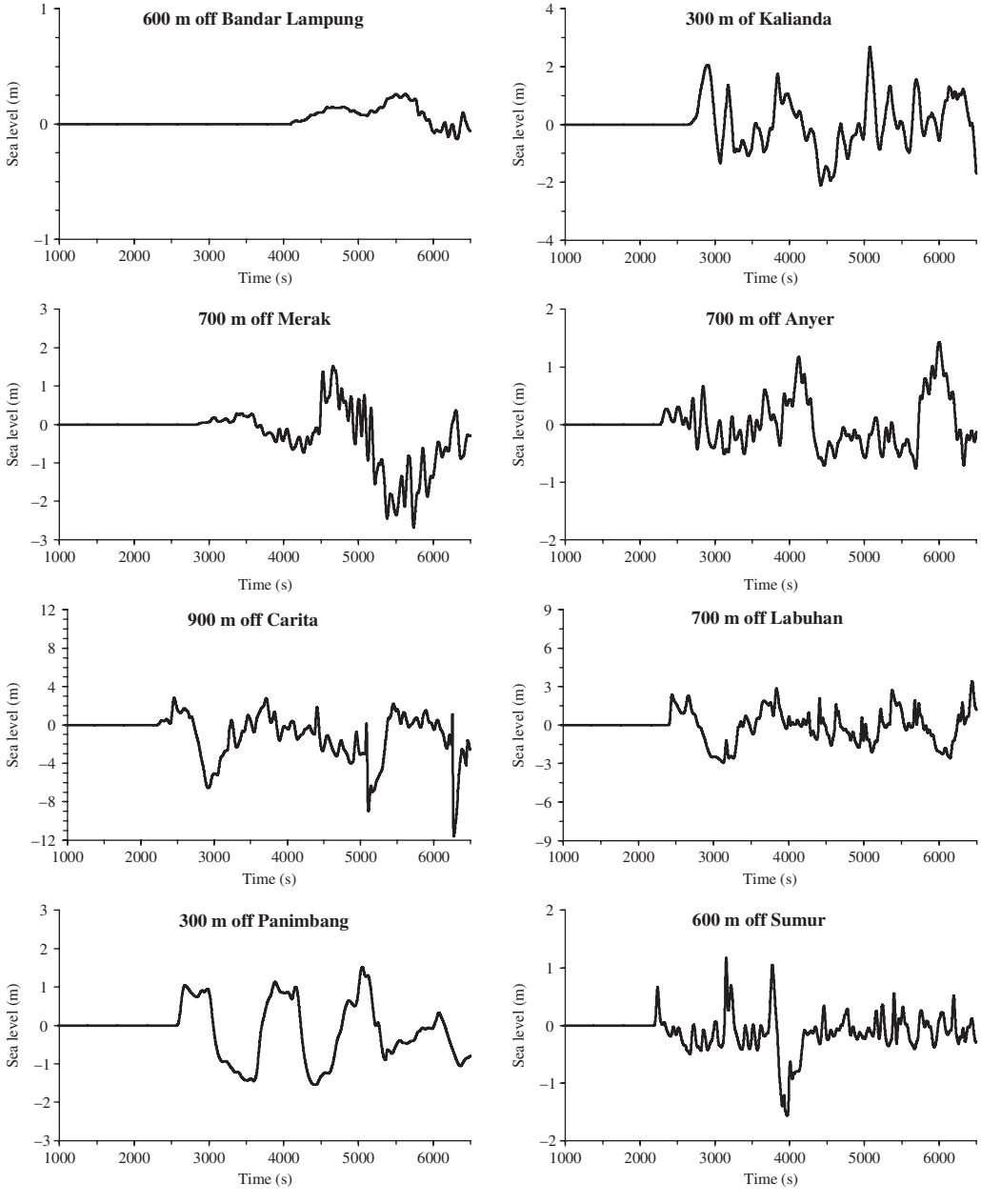

Fig. 6. Simulated sea-level profiles (m) registered several hundred metres (indicated on the plots) off eight of the main coastal cities located in Figure 1. The simulation of the landslide propagation was carried out using a constant retarding stress of 10 kPa. Time is expressed in seconds after the collapse onset. The water depth below each gauge is indicated in Table 1.

improve the accuracy when defining the initial conditions of the landslide. Side-scan sonar surveys coupled with INSAR (Interferometric Synthetic Aperture Radar) monitoring may also reveal evidence of slope instability. The travel time map of the first wave based on the simulations (Fig. 4) is consistent with the refraction diagram of the tsunami caused by the 1883 Krakatau eruption (Yokoyama 1981). However, the wave travel time estimated may suffer from artefacts in the

bathymetry used for calculations. The inclusion of bathymetric maps of parts of Sunda Strait in the constructed DEM allowed us to minimize these artefacts, but new bathymetric maps of this region would be useful for a better tsunami hazard assessment.

Tsunami hazards

Our simulation shows that the first wave produced has a maximum amplitude of about 45 m. This height is reached at approximately 2.5 km SW of the landslide scar (i.e. Anak Krakatau Island), inside the Krakatau Archipelago. Moreover, the waves produced reach the surrounding islands of Sertung, Rakata and Panjang in less than 1 min, with heights of up to 30 m. These waves could be a serious hazard for the many tourist boats that visit these islands every day. Further from the Krakatau Archipelago, the wave amplitude decreases in Sunda Strait and waves are generally smaller than 10 m at a distance of more than 20 km from the landslide scar. However, these waves could still be dangerous for the small boats crossing the strait between the Krakatau Archipelago and the coasts of Java or Sumatra. It should be noted that the islands of the Krakatau Archipelago (Anak Krakatau, Sertung, Panjang and Rakata), as well as those of Sebesi and Sebuku in the NE, those of Legundi and Siuntjal in the NNW, and Panaitan in the SSW are uninhabited, and thus the risk is drastically reduced. Between the two islands of Java and Sumatra, where the planned bridge is to be constructed (see the explanation in the earlier section on 'Geography, population and infrastructures in the Sunda Strait'), the waves do not reach more than 3.8 m, and the construction should be able to absorb the strain developed by such a wave.

Our numerical simulation of the sudden collapse of Anak Krakatau Volcano into the 1883 caldera shows that all the coasts around the Sunda Strait could potentially be affected by waves of more than 1.0 m in less than 1 h after the event. Even the southern coasts of Sumatra, which are located more than 40 km to the north of the landslide, would be touched by the tsunami because of the numerous wave reflections off the islands of the Krakatau Archipelago. All of the main cities or infrastructures of the Sunda Strait would be affected within 1 h of the collapse. The highest waves registered off these coastal cities are those near Labuhan (3.4 m) on the western coast of Java, but most of the gauges give values of less than 3 m for the highest wave. These values are far less than those observed during the 1883 Krakatau eruption, which reached an average value of 15 m on the coasts of Sumatra and Java (Symons 1888; Yokoyama 1981), with a local wave height of up to 30 m. Moreover, Figure 5 shows that some parts of the coast are partially protected by the numerous islands in Sunda Strait (e.g. Rakata prevents the propagation of very high waves towards the large bay off Panimbang). Waves become smaller with increasing distance from the triggering event. During the 1883 tsunami, Jakarta was touched by a wave approximately 1.8 m high about 140 min after the eruption of Krakatau, whereas Merak and Anyer were touched by 15 m-high waves. Likewise, the 1883 tsunami also reached locations thousands of kilometres from the volcano (Choi *et al.* 2003, Pelinovsky *et al.* 2005). Considering that the maximum wave height recorded off Anyer and Merak is around 1.5 m in our simulation, we believe that the tsunami triggered by a flank collapse at Anak Krakatau would be negligible at Jakarta.

Conclusion

Our numerical simulation shows that a partial destabilization (0.28 km^3) of Anak Krakatau Volcano towards the SW would possibly be dangerous on a local scale (tourist and fishing activities around the volcano) or even on a regional scale (coasts of Sumatra and Java). This event would trigger an initial wave of 43 m that would reach all of the islands in the Krakatau Archipelago in less than 1 min, with amplitudes ranging from 15 to 30 m, and would be extremely dangerous for boats in the Krakatau Archipelago. Waves would then propagate in a radial manner across Sunda Strait at an average speed of 80–110 km h^{-1}, the first wave reaching cities on the western coast of Java after 35–45 min, with a maximum amplitude of between 2.9 (Carita) and 3.4 m (Labuhan). These waves would be considerably smaller than those produced during the 1883 Krakatau eruption (average wave height of *c.* 15 m around the Sunda Strait).

Owing to the high population, the concentration of road and industrial infrastructure along some parts of the exposed coasts of Java and Sumatra, and the low elevation of much of this land, the tsunami might present a significant risk. However, as the travel time of the tsunami is several tens of minutes between the Krakatau Archipelago and the main cities along these coasts, a rapid detection of the collapse by the volcano observatory, coupled with an efficient alert system on the coast, could prevent this hypothetical event from being deadly. A tsunami preparedness project was initiated in 2006 by UNESCO and the Indonesian Institute of Sciences (LIPI). However, it should be noted that the ground deformation of the volcano is not permanently monitored, and the available data (e.g. bathymetry) are not sufficient to allow for an accurate assessment of slope instability.

The example of Krakatau Volcano illustrates the point that tsunamis generated by volcanic eruptions and flank instability are a neglected hazard. They represent 25% of all the fatalities directly attributable to volcanoes during the last 250 years (Latter 1981; Begét 2000). At least 115 volcanic tsunamis have been observed since 1600 AD (death toll >54 000), with 36 events during the nineteenth century and 54 events during the twentieth. Volcanic tsunamis can be dangerous because they can occur with little warning, and cause devastation at great distances. South Asian and South Pacific regions are particularly exposed to volcanic tsunamis because of the high density of active volcanoes located near the coasts (volcanic island arcs). Systematic monitoring of flank instability and the integration of tsunamis into volcanic hazard assessments (e.g. maps, evacuation routes) would reduce the impact of future events.

This work is part of the 'Vitesss' project (Volcano-Induced Tsunamis: numErical Simulations and Sedimentary Signature) supported by the French National Research Agency (ANR project 08-JCJC-0042) and whose leader is R. Paris (Geolab, CNRS). ASTER GDEM is a product of METI and NASA. We thank two anonymous reviewers for their constructive reviews of this manuscript. We are also grateful to Anaïs Ferot who first suggested we perform this study.

References

Begét, J. E. 2000. Volcanic tsunamis. *In*: Sigurdsson, H., Houghton, B., McNutt, S. R., Rymer, H. & Stix, J. (eds) *Encyplopedia of Volcanoes*. Academic Press, New York, 1005–1013.

Camus, G. & Vincent, P. M. 1983. Discussion of a new hypothesis for the Krakatau volcanic eruption in 1983. *Journal of Volcanology and Geothermal Research*, **19**, 167–173.

Camus, G., Gourgaud, A. & Vincent, P. M. 1987. Petrologic evolution of Krakatau (Indonesia): implications for a future activity. *Journal of Volcanology and Geothermal Research*, **33**, 299–316.

Carey, S., Sigurdsson, H., Mandeville, C. W. & Bronto, S. 1996. Pyroclastic deposits from flows and surges which travelled over the sea during the 1883 eruption of Krakatau volcano. *Bulletin of Volcanology*, **57**, 493–511.

Casalbore, D., Romagnoli, C., Bosman, A. & Chiocci, F. L. 2011. Potential tsunamigenic landslides at Stromboli Volcano (Italy): insight from marine DEM analysis. *Geomorphology*, **126**, 42–50, doi: 10.1016/j.geomorph.2010.10.026.

Choi, B. H., Pelinovsky, E., Kim, K. O. & Lee, J. S. 2003. Simulation of the trans-oceanic tsunami propagation due to the 1883 Krakatau volcanic eruption. *Natural Hazards and Earth System Sciences*, **3**, 321–332.

Dade, W. B. & Huppert, H. E. 1998. Long-runout rockfalls. *Geology*, **26**, 803–806.

de Lange, W. P., Prasetya, G. S. & Healy, T. R. 2001. Modelling of tsunamis generated by pyroclastic flows (ignimbrites). *Natural Hazards*, **24**, 251–266.

Deplus, C., Bonvalot, S., Dahrin, D., Diament, M., Harjono, H. & Dubois, J. 1995. Inner structure of the Krakatoa volcanic complex (Indonesia) from gravity and bathymetry data. *Journal of Volcanology and Geothermal Research*, **64**, 23–51.

Francis, P. W. 1985. The origin of the 1883 Krakatau tsunamis. *Journal of Volcanology and Geothermal Research*, **25**, 349–363.

Fritz, H. M., Hager, W. H. & Minor, H. E. 2001. Lituya Bay case: rockslide impact and wave run-up. *Science of Tsunami Hazards*, **19**, 3–22.

Fritz, H. M., Kalligeris, N. J., Borrero, C., Broncano, P. & Ortega, E. 2008. The 15 August 2007 Peru tsunami runup observations and modeling. *Geophysical Research Letters*, **35**, L10604-4, doi: 10.1029/2008GL033494.

Giachetti, T., Paris, R., Kelfoun, K. & Pérez-Torrado, F. J. 2011. Numerical modelling of the tsunami triggered by the Güìmar debris avalanche, Tenerife (Canary Islands): comparison with field-based data. *Marine Geology*, **284**, 189–202, doi:10.1016/j.margeo.2011.03.018.

Harbitz, C. B., Løvholt, F., Pedersen, G. & Masson, D. G. 2006. Mechanisms of tsunami generation by submarine landslides: a short review. *Norwegian Journal of Geology*, **86**, 255–264.

Hoffmann-Rothe, A., Ibs-von Seht, M. *et al.* 2006. Monitoring Anak Krakatau Volcano in Indonesia. *Eos Transactions of the American Geophysical Union*, **87**, 581, doi: 10.1029/2006EO510002.

Keating, B. H. & McGuire, W. J. 2000. Island edifice failures and associated tsunami hazards. *Pure and Applied Geophysics*, **157**, 899–955.

Kelfoun, K. & Druitt, T. H. 2005. Numerical modelling of the emplacement of Socompa rock avalanche, Chile. *Journal of Geophysical Research*, **110**, B12202.

Kelfoun, K., Giachetti, T. & Labazuy, P. 2010. Landslide-generated tsunamis at Reunion Island. *Journal of Geophysical Research*, **115**, F04012, doi: 10.1029/2009JF001381.

Latter, J. N. 1981. Tsunamis of volcanic origin: summary of causes with particular references to Krakatoa, 1883. *Bulletin of Volcanology*, **44**, 467–490.

Locat, J., Lee, H. J., Locat, P. & Irman, J. 2004. Numerical analysis of the mobility of the Palos Verdes debris avalanche, California, and its implication for the generation of tsunamis. *Marine Geology*, **203**, 269–280.

Mader, C. L. & Gittings, M. L. 2006. Numerical model for the Krakatoa hydrovolcanic explosion and tsunami. *Science of Tsunami Hazards*, **24**, 174–182.

Maeno, F. & Imamura, F. 2007. Numerical investigations of tsunamis generated by pyroclastic flows from the Kikai caldera, Japan. *Geophysical Research Letters*, **34**, L23303-1, doi: 10.1029/2007GL031222.

Maeno, F., Imamura, F. & Taniguchi, H. 2006. Numerical simulation of tsunami generated by caldera collapse during the 7.3 ka Kikai eruption, Japan. *Earth Planets and Space*, **58**, 1013–1024.

MARAMAI, A., GRAZIANI, L. *ET AL.* 2005. Near- and far-field survey report of the 30 December 2002 Stromboli (Southern Italy) tsunami. *Marine Geology*, **215**, 93–106.

MICHIUE, M., HINOKIDANI, O. & MIYAMOTO, K. 1999. Study on the Mayuyama tsunami disaster in 1792. *In*: *Proceedings of the 28th IAHR Congress, Graz, Austria, 22–27 August 1999*. International Association of Hydro-Environment Engineering and Research, Madrid (CD-ROM).

NOMANBHOY, N. & SATAKE, K. 1995. Generation mechanism of tsunamis from the 1883 Krakatau eruption. *Geophysical Researc. Letters*, **22**, 509–512.

OBA, N., TOMITA, K. *ET AL.* 1983. Geochemical study of volcanic products, in particular to pumice flow, of the Krakatau Group, Indonesia. *Report of the Faculty of Science, Kagoshima University (Earth Science, Biology)*, **16**, 21–41.

PELINOVSKY, E., CHOI, B. H., STROMKOV, A., DIDENKULOVA, I. & KIM, H. S. 2005. Analysis of tide-gauge records of the 1883 Krakatau tsunami. *In*: *Tsunamis: Case Studies and Recent Developments. Advances in Natural and Technological Hazards Research*, **23**, 57–77.

SELF, S. & RAMPINO, M. R. 1981. The 1883 eruption of Krakatau. *Nature*, **294**, 699–704.

SIGURDSSON, H., CAREY, S. & MANDEVILLE, C. 1991*a*. Submarine pyroclastic flows of the 1883 eruption of the Krakatau Volcano. *National Geographic Research and Exploration*, **7**, 310–327.

SIGURDSSON, H., CAREY, S., MANDEVILLE, C. & BRONTO, S. 1991*b*. Pyroclastic flows of the 1883 Krakatau eruption. *Eos Transactions of the American Geophysical Union*, **72**, 377.

SIMKIN, T. & FISKE, R. S. 1983. *Krakatau 1883: The Volcanic Eruption and its Effects*. Smithsonian Institution Press, Washington, DC.

STEHN, C. E. 1929. The geology and volcanism of the Krakatau Group. *In*: *Proceedings of the Fourth Pacific Science Congress, Batavia-Bandoeng (Java), May–June, 1929*. Martinus Nijhoff, The Hague, 1–55.

SUDRADJAT, A. 1982. The morphological development of Anak Krakatau Volcano, Sunda Strait. *Geology of Indonesia*, **9**, 1–11.

SYMONS, G. J. 1888. *The Eruption of Krakatoa, and Subsequent Phenomena. Report of the Krakatoa Committee of the Royal Society*. Trübner, London.

SYNOLAKIS, C. E., LIU, P. L. F., YEH, H. & CARRIER, G. F. 1997. Tsunamigenic seafloor deformations. *Science*, **278**, 598–600.

TINTI, S., BORTOLUCCI, E. & ROMAGNOLI, C. 1999. Modelling a possible holocenic landslide-induced tsunami at Stromboli volcano, Italy. *Physics and Chemistry of the Earth*, **24**, 423–429.

TINTI, S., BORTOLUCCI, E. & ROMAGNOLI, C. 2000. Computer simulations of tsunamis due to sector collapse at Stromboli, Italy. *Journal of Volcanology and Geothermal Research*, **96**, 103–128.

TINTI, S., PAGNONI, G. & ZANIBONI, F. 2006. The landslides and tsunamis of the 30th of December 2002 in Stromboli analysed through numerical simulations. *Bulletin of Volcanology*, **68**, 462–479.

TSUJI, Y. & HINO, T. 1993. Damage and inundation height of the 1792 Shimabara landslide tsunami along the coast of Kumamoto prefecture. *Bulletin of the Earthquake Research Institute, University of Tokyo*, **68**, 91–176.

VERBEEK, R. D. M. 1885. Krakatau. *In*: SIMKIN, T & FISKE, R. S (eds) *Krakatau 1883: The Volcanic Eruption and its Effects*. Smithsonian Institution Press, Washington, DC, 169–277.

WARD, S. N. 2001. Landslide tsunami. *Journal of Geophysical Research*, **106**, 11 201–11 215.

WARD, S. N. & DAY, S. 2003. Ritter Island Volcano-lateral collapse and the tsunami of 1888. *Geophysical Journal International*, **154**, 891–902.

WAYTHOMAS, C. F., WATTS, P., SHI, F. & KIRBY, J. T. 2009. Pacific Basin tsunami hazards associated with mass flows in the Aleutian arc of Alaska. *Quaternary Science Reviews*, **28**, 1006–1019.

WARTON, W. J. L. & EVANS, F. J. 1888. On the seismic sea waves caused by the eruption at Krakatoa, August 26th and 27th, 1883. Part III. *In*: SYMONS, G. L. (ed.) *The Eruption of Krakatoa and Subsequent Phenomena*. Report of the Krakatoa Commission of the Royal Society of London, 89–151.

YOKOYAMA, I. 1981. A Geophysical interpretation of the 1883 Krakatau eruption. *Journal of Volcanology and Geothermal Research*, **9**, 359–378.